A-site cation controlled localization of dipole correlations in a relaxor material

Jiahao Zhang [●],[1] Drew Behrendt [●],[1] Yubo Qi,[2] and Andrew M. Rappe [●][1]

[1]*Department of Chemistry, University of Pennsylvania, Philadelphia, Pennsylvania 19104-6323, USA*
[2]*Department of Physics, University of Alabama at Birmingham, Birmingham, Alabama 35233, USA*

In this work, we carry out molecular dynamics simulations based on an extended version of the bond valence force field to investigate the underlying physics of relaxor dielectrics with static temperature-stable dielectric response. We focus on the perovskite solid solution $(1 - x)\mathrm{Ba_{0.95}Ca_{0.05}TiO_3} - (x)\mathrm{Bi_{0.5}MeO_3}(\mathrm{Me} = \mathrm{Mg_{1/2}Ti_{1/2}}, \mathrm{Sc}, \mathrm{Zn_{1/2}Ti_{1/2}})$, which has a flat dielectric response over a wide temperature range which was recently observed experimentally. Our molecular dynamics simulations can not only reproduce the temperature-dielectric relationship observed in experiments, but also provide an atomic scale explanation. Specifically, doping $\mathrm{Bi(Mg_{1/2}Ti_{1/2})O_3}$ into the $\mathrm{(BaCa)TiO_3}$ crystal reduces the spatial correlation length of electric dipole orientations to the minimum distance, which is only within the neighboring unit cells. This nearest-neighbor correlation even persists at high temperatures. As a result, in this perovskite solid solution, the correlation length and macroscopic polarization change little with the temperature, leading to temperature-stable relaxor dielectric responses. The relationships between our theory and previously proposed models, such as the independent local mode and correlated rattling cations model, are also discussed. This theoretical work aims to deepen our understanding of the theory of connecting between atomic composition and temperature-stable relaxor dielectric response.

I. INTRODUCTION

The dielectric constant measures the first-order change of polarization with an external electrical field. In a conventional perovskite ferroelectric, such as $\mathrm{PbTiO_3}$ or $\mathrm{BaTiO_3}$, the dielectric constant is strongly temperature dependent and has sharp peaks at the temperatures under which phase transitions occur. However, a relaxor ferroelectric, with disordered chemical doping, has a diffuse phase transition and a much smoother change of dielectric constant with temperature [1–3]. In prototypical relaxors, such as $\mathrm{Ba(Zr_{1/2}Ti_{1/2})O_3}$ (BZT) and $(0.75)\mathrm{PbTiO_3}$-$(0.25)\mathrm{Pb(Mg_{1/3}Nb_{2/3})O_3}$ (PMN-PT), the dielectric response is high magnitude over a wide temperature range, giving them numerous military and industrial applications such as capacitors and transducers [1,4–14].

The unique properties of relaxors have attracted intense research interest. Due to their intrinsic complexity, relaxor systems have been described as a "hopeless mess" [15]. However, recent developments in computational techniques, especially molecular dynamics based on bond-valence models, enable large-scale simulations that have provided deep insights into the relaxor behavior [9,16,17]. Specifically, the slushlike polar nanodomain (PND) model was recently proposed to explain the relaxor behavior in PMN-PT. In this model, a relaxor structure is composed of nanodomains, which transit from fully frozen domains to a mixture of frozen and dynamic ones, and finally to fully dynamic domains as temperature increases [11]. It can be useful to view each nanodomain as having a distinct phase transition temperature, leading to a large and smooth dielectric constant over a large temperature range, rather than an infinite dielectric response at one curie temperature. However, there is a temperature (denoted as $T_{\max}$) at which a long-range correlation is more likely to transform into short-range correlations, corresponding to the breakup of a large frozen polar domain into several dynamic domains. The dielectric response peaks at this temperature, which inspires the search for a new type of relaxor with even greater temperature stability of its dielectric response [18,19].

There is an immense desire for temperature-stable relaxor dielectrics (TSRDs), which have promising applications in devices with robust temperature stability; designing and searching for TSRDs have inspired intense research interest that has led to great progress. For example, recent experimental studies showed that doping $\mathrm{BiMeO_3}$ into $\mathrm{BaTiO_3}$ [where $\mathrm{Me} = \mathrm{Mg_{1/2}Ti_{1/2}}, \mathrm{Sc}, \mathrm{Zn_{1/2}Ti_{1/2}}$] can induce a stable dielectric response over a wide temperature range [18–22]. Several models have been proposed to understand the temperature-stable dielectric response [18,20,23]. For example, in the correlated rattling cations (CRC) model, A-site and B-site atoms are assumed to have coupled rattling motions [23,24]. The CRC model was determined by the reverse Monte Carlo method in order to reproduce the observed physical quantities, such as pair distribution functions and scattering signals, experimentally. The rattling coupling was found to be short range for a wide range of temperatures, leading to temperature-stable polarization fluctuations and dielectric responses. In the independent local mode (ILM) model, the transverse optical mode, which is soft originally, is hardened by Sc or Bi substitutions [18]. As a result, the large dielectric responses induced by phase transitions are suppressed [18]. Both of these models are built on direct observations from experiments. A complete independent atomistic understanding of stable dielectric response is needed.
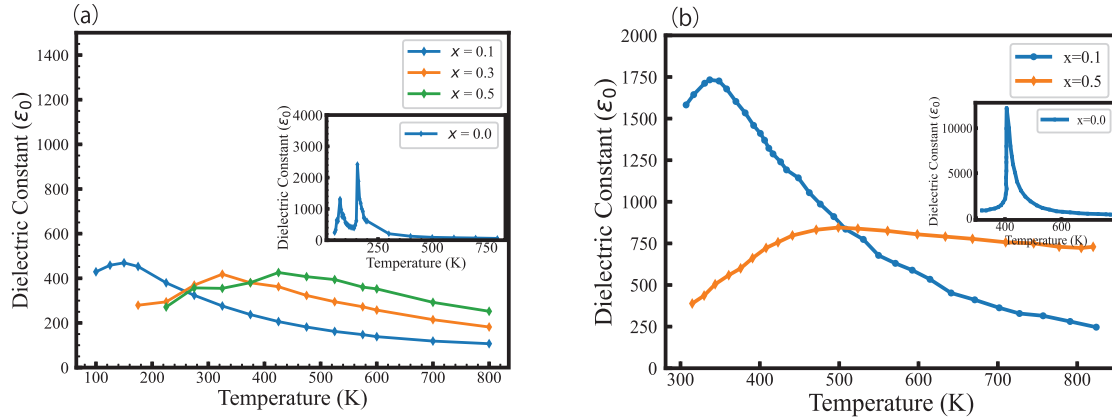
FIG. 1. Dielectric constants of $(1-x)$BCT-(x)BMT as a function of temperature. (a) Theory calculations. (b) Experimental results of 1MHz dielectric response taken from Ref. [49]. As x increases, the dielectric constant curves get flatter, indicating the transition from conventional ferroelectrics to TSRDs.

In this paper, we use molecular dynamics (MD) simulations fitted to first-principle results to investigate the origin of flat dielectric vs temperature. We compare our MD simulations with previous experiments and provide an atomistic explanation of both the CRC and ILM models. Overall, we aim to provide both physical insights into the TSRD response and guidance to enable creative material design of future TSRD for various applications.

II. METHODS

The MD simulations are performed based on the bond-valence MD (BVMD) model [25–33]. Detailed descriptions and parameters of the model are described in the Supplemental Material (SM) [34]. MD simulations are conducted using LAMMPS, with 1 femtosecond as the time step [35]. The parameters for the force field are fitted based on a database that consists of DFT calculations of 5000 structures. The DFT calculations are carried out with the Quantum Espresso package [36] with the modified Perdew-Burke-Ernzerh exchange-correlation functional for solids (PBEsol) [37]. The norm-conserving pseudopotentials are generated with the OPIUM package [38–40]. We used 50 Ry for plane wave cutoff, and $4 \times 4 \times 4$ Monkhorst-Pack k-point mesh for integration over the Brillouin zone [41].

III. RESULTS

To test the performance of our force field, we begin with calculating the static composition-dependent dielectric constant of $(1-x)$Ba$_{0.95}$Ca$_{0.05}$TiO$_3$-(x) BiMg$_{1/2}$Ti$_{1/2}$O$_3$ (BCT-BMT) and compare theoretical simulations with experimental results. We perform isobaric–isothermal ensemble (NPT) MD simulations with the pressure fixed at 1 atm with the Parrinello-Rahman barostat [42]. The temperature is controlled via the Nosé-Hoover thermo-stat with thermal inertia parameter Ms set as 1.0 atomic unit [43,44]. At each temperature for relaxor material, we find that running for 150 000 steps (0.15 ns) is enough for the system to reach an equilibrium state, after which we run another 1 000 000 steps (1.0 ns) to keep track of the polarization fluctuations. The

static dielectric constant is calculated with the Green-Kubo formula [45–47]:

$$\epsilon(0) - 1 = \frac{V}{3\epsilon_0 k_B T} \langle \delta \vec{P}(t)^2 \rangle.$$ (1)

Here, k_B is the Boltzmann constant, T is the temperature, V is the volume, $\vec{P}(t)$ is the polarization magnitude at time t, and ϵ_0 is the permittivity of free space. The polarization is calculated by

$$\vec{P} = \frac{1}{V} \sum_n (\mathbf{Z}_{\mathbf{n,A}}^* \cdot \vec{r}_{n,A} + \mathbf{Z}_{\mathbf{n,B}}^* \cdot \vec{r}_{n,B} + \mathbf{Z}_{\mathbf{n,O}}^* \cdot \vec{r}_{n,O}).$$ (2)

Here, $\mathbf{Z}_{\mathbf{n,\cdot}}^*$ denotes the Born effect charge of the atom at the A, B, or O site in a perovskite structure, and its value is acquired through first-principles calculations [48].

The calculated concentration-dependent dielectric constants for BCT-BMT are shown in Fig. 1, which are in good agreement with experimental measurement [50]. At $x = 0.0$ (nondoped, traditional ferroelectric regime), the dielectric constant curve peaks at 80 K and 175 K, which correspond to the rhombohedral-to-tetragonal and tetragonal-to-cubic phase transitions (Here, the orthorhombic phase is much suppressed due to the Ca doping) [33]. This is because, at the phase transition temperature, at least one of the polarization components (P_x, P_y, or P_z) fluctuates between zero and a finite value, leading to a divergence in polarization fluctuation and an infinite dielectric constant. When a ferroelectric material is selectively doped, relaxor properties can emerge, and the phase transition becomes localized rather than perfectly uniform across the entire crystal; each local domain has its distinctive dynamics and phase transition temperature [9,11,51]. As a result, the dielectric constant curve becomes broader and diffuses rather than peak at a specific temperature [11].

As indicated by the Kubo-Green formula, the dielectric constant depends on the fluctuation of macroscopic polarization, which is determined by the spatial correlation between local dipoles. Such a spatial correlation between unit cells can be described by the dipole correlation angle as [11]

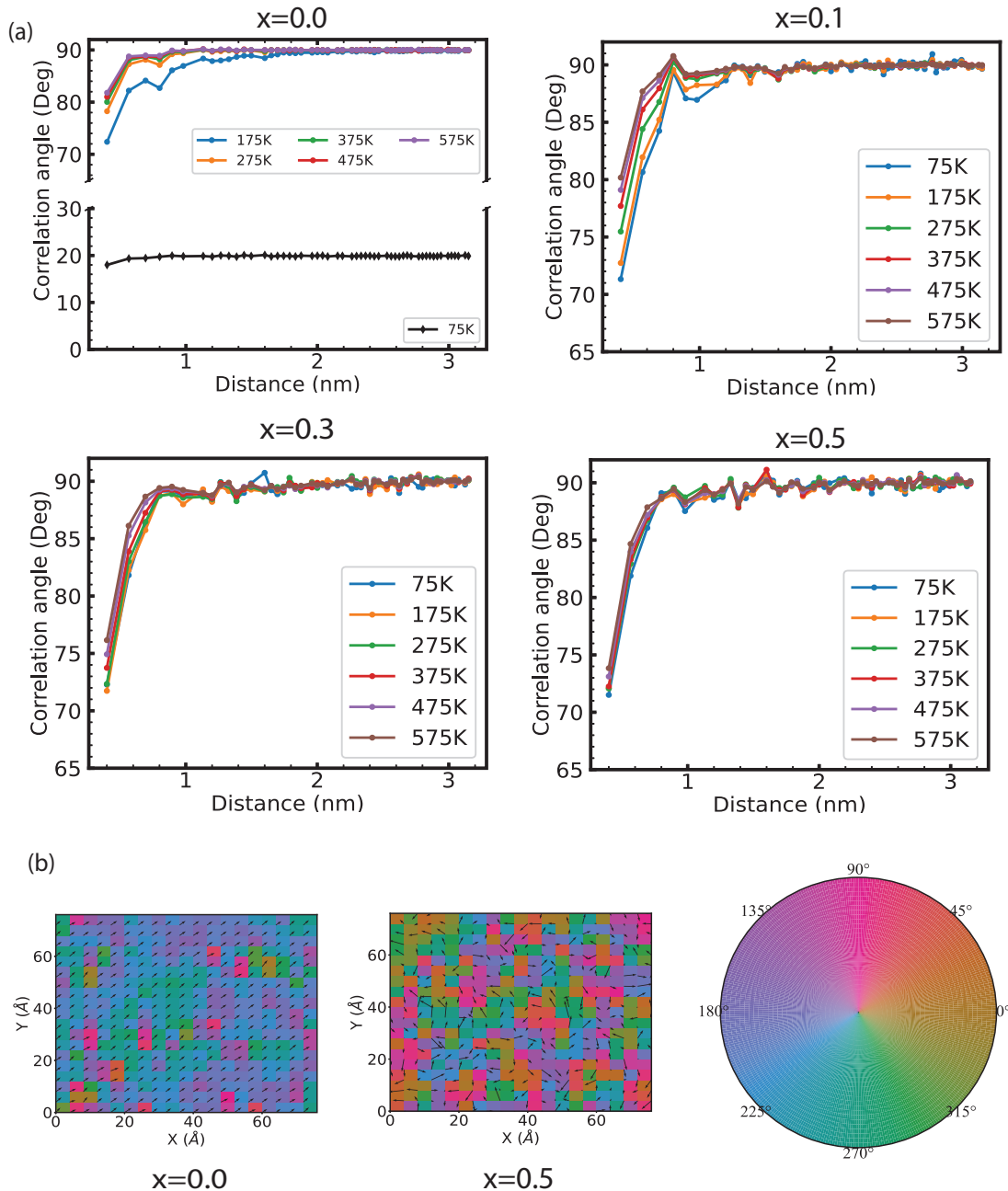$$\theta(r) = \arccos\left(\langle \hat{P}(r_0, t) \cdot \hat{P}(r_0 + r, t) \rangle_{r_0, t}\right).$$ (3)

FIG. 2. Spatial correlation function of (1-x)BCT - xBMT. (a) Change of the spatial-correlation angle with distance in (1-x)BCT- xBMT as a function of x. As x increases, the alloy system goes from a long-range correlation ferroelectric material into relaxor with a short-range correlation that's sensitive to temperature. Finally, it entered a relaxor dielectric phase in which the correlation function is insensitive to temperature. For x=0.0, the material goes through a ferroelectric phase transition, as shown in Fig. 1. As a result of the ferroelectric phase transition, the long-range aligned dipole disappeared, while short-range alignment still exists. The phase transition temperature from tetragonal to cubic is 160 K in the simulation [33]. (b) A snapshot of the polarization profile in (1-x)BCT- x BMT when $x = 0.0$ and 0.5. The color panel represents the radial angle of the in-plane polarization direction.

For a purely ferroelectric material, the spatial correlation spans the entire material. On the other hand, in a relaxor, compositional disorder breaks the long-range correlation. As shown in Fig. 2(a), for pure BCT, the material is a ferroelectric with a long-range correlation at temperatures below T_C [49]. When temperature increases, the long-range correlation disappears, indicating a ferroelectric-to-paraelectric phase transition. It is worth noting that even in the

paraelectric state, each unit cell in BCT still has a nonzero and time-dependent dipole. This is because the transition exhibits a mixture of order-disorder and displacive characters [33]. Moreover, the short-range correlations between neighboring unit cells persist above T_C but decrease as temperature increases.

The last three figures of Fig. 2(a) shows the changes of dipole correlation angle with distance at different
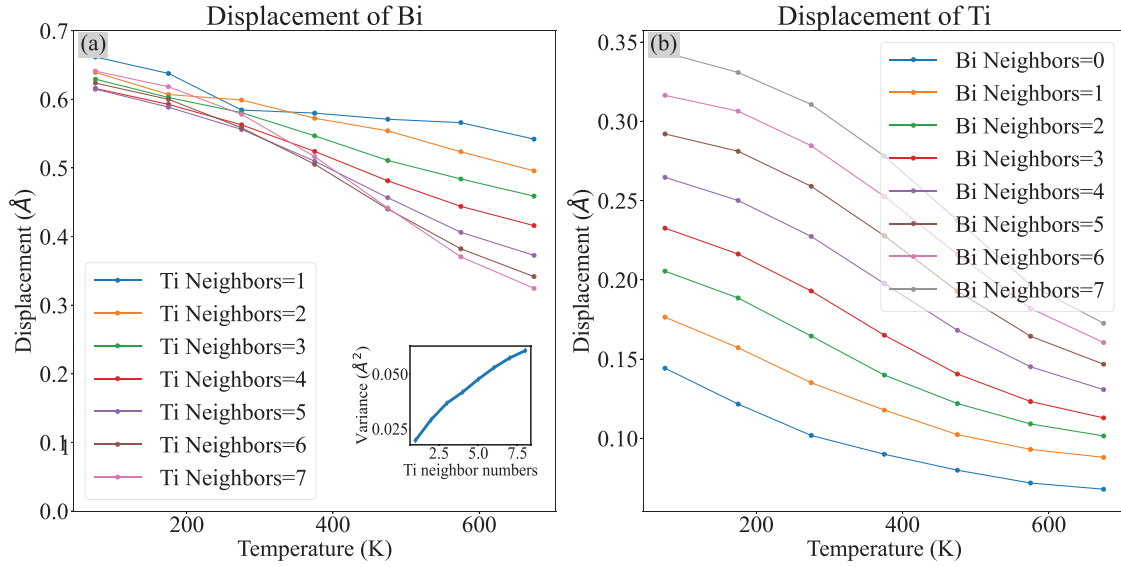
FIG. 3. Displacements of Bi and Ti atoms at various neighboring environments. The displacements of Ti and Bi are defined as distance from oxygen octahedral and oxygen cuboctahedron, respectively. (a) Displacements of Bi atoms under Ti environment. The low-temperature displacements of Bi are not sensitive to the neighboring Ti environments. The lower right figure shows the position variance of Bi atoms at 475 K. Ti neighbors at high temperature increase the mobility of Bi due to the local random force, thus resulting in less net displacement. (b) Displacement of Ti atoms are positively correlated to the local coordination of Bi. The displacements of Ti atoms are strongly controlled by neighboring Bi numbers. This is due to the fact that Bi atoms have larger ferroelectric displacement compared to Ti atoms. And Bi related ferroelectrics like $BiFeO_3$ have a much larger curie temperature compared to Ti based ferroelectric materials like $BaTiO_3$ indicating ferroelectricity in Bi related materials are more thermodynamically stable compared to Ti counterparts[30,33,55–58]. The displacement of A-site and B-site atoms in perovskite cations are coupled with each other [59].

temperatures when doped with BMT. There are two important features. First, there is no long-range correlation at any temperature. For the distances r equal to or greater than two unit cells (1 nm), the dipole correlation angle θ is larger than 85°, indicating little interaction. This is dramatically different from conventional (non-temperature-stable) relaxors, such as PMN-PT. In PMN-PT, large domains are likely to break into smaller ones at temperatures around T_{max}, leading to a larger polarization variance and higher dielectric constant. In BCT-BMT, the dipole correlations are mostly short-range, indicating that increasing temperature does not change the sizes of domains much, which is essential for a temperature-stable dielectric constant. Here, the correlation is almost completely within only the nearest neighbor, which we refer to as the intrinsic correlation limit. Another feature is that the dipole correlation angle values do not change much with temperature, indicating that the nearest-neighbor coupling is strong and temperature insensitive. This is consistent with previous experimental observations of nearly insensitive domain distribution upon varying temperature [24]. In the following parts, we will discuss the underlying reasons for these two features, which jointly lead to the temperature-stable dielectrics, based on an atomic-scale analysis.

The A-site doped Bi atoms influence the dynamics of a B-site Ti atom, whose displacement has a significant contribution to the polarization of a cell. A Bi dopant, as a lower concentration substitution at A-site, can induce a strong local distortion, making the neighboring Ti atoms have preferred distortions and unlikely to hop between different equivalent displaced sites. In other words, doping Bi can make the originally soft transverse optical mode more damped as a result of

asymmetrical double well potential and local random forces [52], and the extent of vibration and displacement of a Ti atom depends on the number of its neighboring Bi atoms. As shown in Fig. 3, the Ti atoms having more neighboring Bi atoms are more displaced at any temperature. For different times t, we calculate the time-dependent auto correlation function $\phi(t) = \langle \vec{D}(\tau) \cdot \vec{D}(t + \tau) \rangle_\tau$ of different unit cells [9]. Here, $\vec{D}(t)$ is the atomic displacement at time t. The relaxation time is defined as the average time when the correlation reduces to 1 e of its initial value $\phi(t = 0)$. The shorter relaxation time indicates shorter local memory [9]. Figure 4(a) shows distributions of relaxation time for Ti atoms with different numbers of Bi neighbors. Consistent with our analysis, the more Bi neighbors a Ti atom has, the longer the relaxation time is. Ti neighboring also has a similar effect on the dynamics of Bi atoms by slightly decreasing the relaxation time of Bi atoms, as shown in Fig. 4(b). These results indicate that Bi doping breaks the long-range coupling; the dynamics of a Ti atom depends mostly on the number of Bi neighbors, rather than on the dynamics of its neighboring Ti atoms.

It is worth mentioning that the breaking of long-range interactions by local chemical composition variation also exists in prototype relaxors, such as PMN-PT. Specifically, B-site doped Mg atoms change local structures (under-bonded Oxygen atoms) and thus, weaken the long-range interaction. However, the extent of weakening is less compared with that in a TSRD, such as BCT-BMT, for the following reasons. First, the A-site substitution in BCT-BMT leads to a strong intracell A-B-site interaction, which is expected to be stronger than the intercell B-B-site interaction in PMN-PT. Second, the mismatch between the ionic size of the original atom and
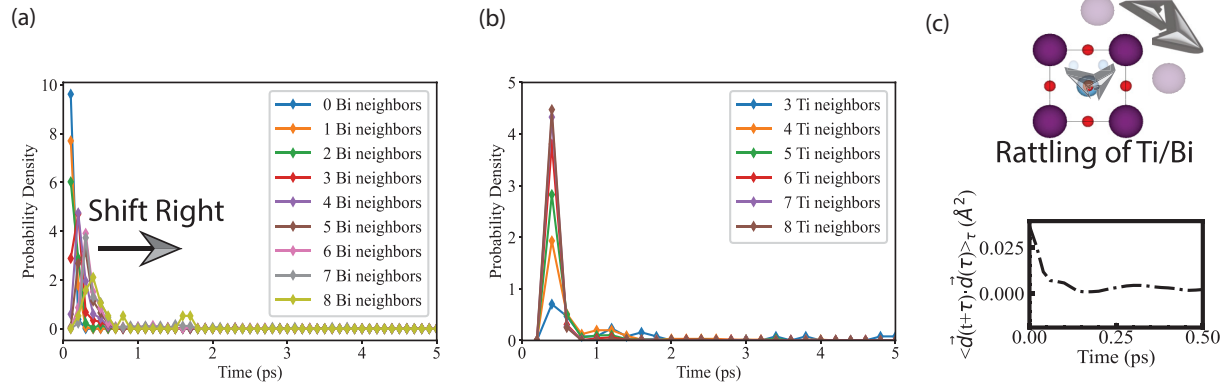
FIG. 4. (a) Distribution of the relaxation time of Ti atoms at 875 K with different numbers of Bi neighbors. The relaxation time of Ti atoms are strongly affected by the neighboring Bi atoms coordination. The more Bi coordination results in longer relaxation time. (b) Distribution of the relaxation time of Bi atoms with different numbers of Ti neighbors at 875 K. The more Ti neighbors will slightly reduce the Bi relaxation time, which is a result of active motions of surrounding Ti neighbors. The effects are more evident at high temperature. (c) Definition of relaxation time as the time when the auto-correlation function drop to 1 e of the initial value.

that of the dopant is larger in BCT-BMT($r_{Ba} = 1.61$ Å, $r_{Bi} = 1.03$ Å) [53,54], leading to a larger distortion and stronger suppression of long-range correlations. These facts explain why PMN-PT is a relaxor and BCT-BMT is a TSRD.

Our results provide atomic-scale insights into phenomenological CRC and ILM models [18,23,24]. As shown in Figs. 3 and 4, Bi dopants can influence both the displacements and dynamics of Ti atoms, providing theoretical support to the A-B sites coupling in the CRC model. Our analysis also shows that Bi doping suppresses the long-range correlation, making each Ti atom rattle around its most favorable position and couple with only near-site atoms, such as the neighboring A-site atoms. Moreover, our MD simulations observe both larger displacements and longer relaxation times induced by Bi doping, which is consistent with the soft-mode confining in the ILM mode.

displacements and dynamics of atoms within different local chemical environments, we demonstrate that it is the Bi dopants which harden the originally soft Ti-centered modes and also suppress the long-range interactions. This work also provides atomic-level explanations for the independent local mode and correlated rattling cations models, which were phenomenologically proposed to explain experimental observations. This work aims to provide deeper insights into the mechanisms of temperature-stable relaxor dielectrics and thus, inspire future materials designing.

ACKNOWLEDGMENTS

IV. SUMMARY

In summary, we carry out molecular dynamics simulations to investigate the underlying physics of a prototype temperature-stable relaxor dielectric BCT-BMT. Our simulations reveal that the BCT-BMT crystal is composed of small nanodomains with only nearest-neighbor interaction and temperature-insensitive fluctuation. By analyzing the

[1] I. Grinberg, A. Kolpak, Y.-H. Shin, and A. Rappe, Modeling of materials for naval sonar, pollution control, and nonvolatile memory application, in *2007 DoD High Performance Computing Modernization Program Users Group Conference* (2007), pp. 177–184.

[2] R. Cowley, S. Gvasaliya, S. Lushnikov, B. Roessli, and G. Rotaru, Relaxing with relaxors: a review of relaxor ferroelectrics, Adv. Phys. **60**, 229 (2011).

[3] A. A. Bokov and Z.-G. Ye, Dielectric relaxation in relaxor ferroelectrics, J. Adv. Dielect. **02**, 1241010 (2012).

[4] E. Sun and W. Cao, Relaxor-based ferroelectric single crystals: Growth, domain engineering, characterization and applications, Prog. Mater. Sci. **65**, 124 (2014).

[5] S. Zhang, F. Li, J. Luo, R. Sahul, and T. R. Shrout, Relaxor PbTiO$_3$ single crystals forvarious applications, IEEE Trans. Ultrason. Ferroelect. Freq. Contr. **60**, 1572 (2013).

[6] P. Zhao, H. Wang, L. Wu, L. Chen, Z. Cai, L. Li, and X. Wang, Highperformance relaxor ferroelectric materials for energy storage applications, Adv. Energy Mater. **9**, 1803048 (2019).

[7] Y. Yamashita, K. Harada, and S. Saitoh, Recent applications of relaxor materials, Ferroelectrics **219**, 29 (1998).

[8] Y. Chen, K.-H. Lam, D. Zhou, Q. Yue, Y. Yu, J. Wu, W. Qiu, L. Sun, C. Zhang, H. Luo *et al.*, High performance relaxor-based ferroelectric single crystals for ultrasonic transducer applications, Sensors **14**, 13730 (2014).

[9] I. Grinberg, Y.-H. Shin, and A. M. Rappe, Molecular dynamics study of dielectric response in a relaxor ferroelectric, Phys. Rev. Lett. **103**, 197601 (2009).

[10] I. Grinberg, H. Takenaka, Y.-h. Shin, and A. M. Rappe, Prediction of dielectric dispersion for lead based Perovskites and study of dielectric response, J. Adv. Diel. **2**, 1241009 (2012).

[11] H. Takenaka, I. Grinberg, S. Liu, and A. M. Rappe, Slush-like polar structures in single-crystal relaxors, Nature (London) **546**, 391 (2017).

[12] A. R. Akbarzadeh, S. Prosandeev, E. J. Walter, A. Al-Barakaty, and L. Bellaiche, Finite-temperature properties of $Ba(Zr, Ti)O_3$ relaxors from first principles, Phys. Rev. Lett. **108**, 257601 (2012).

[13] K. Uchino and S. Nomura, Critical exponents of the dielectric constants in diffused-phase-transition crystals, Ferroelectrics **44**, 55 (1982).

[14] X. Yan, K. H. Lam, X. Li, R. Chen, W. Ren, X. Ren, Q. Zhou, and K. K. Shung, Correspondence: Lead-free intravascular ultrasound transducer using bzt-50bct ceramics, IEEE Trans. Ultrasonics, Ferroelectrics, and Frequency Control **60**, 1272 (2013).

[15] R. Cohen, Relaxors go critical, Nature (London) **441**, 941 (2006).

[16] M. Sepliarsky and R. E. Cohen, First-principles based atomistic modeling of phase stability in pmn-xpt, J. Phys.: Condens. Matter **23**, 435902 (2011).

[17] M. Sepliarsky, Z. Wu, A. Asthagiri, and R. Cohen, Atomistic model potential for $PbTiO_3$ and pmn by fitting first principles results, Ferroelectrics **301**, 55 (2004).

[18] A. Pramanick, S. Nayak, T. Egami, W. Dmowski, A. S. Budisuharto, F. Marlton, M. R. V. Jørgensen, S. Venkateshwarlu, and K. A. Beyer, Dynamical origins of weakly coupled relaxor behavior in sn-doped $(Ba,Ca)TiO_3BiScO_3$, Phys. Rev. B **103**, 214105 (2021).

[19] A. Zeb and S. Milne, High temperature dielectric ceramics: a review of temperature-stable high-permittivity perovskites, J. Mater. Sci.: Mater. Electron. **26**, 9243 (2015).

[20] H. Ogihara, C. A. Randall, and S. Trolier-McKinstry, Weakly coupled relaxor behavior of $BaTiO_3-BiScO_3$ ceramics, J. Am. Ceram. Soc. **92**, 110 (2009).

[21] N. Raengthon, T. Sebastian, D. Cumming, I. M. Reaney, and D. P. Cann, $BaTiO_3Bi(Zn_{1/2}Ti_{1/2})O_3BiScO_3$ ceramics for high-temperature capacitor applications, J. Am. Ceram. Soc. **95**, 3554 (2012).

[22] M. Cabral, A. Brown, J. Bultitude, A. Britton, R. Brydson, T. Roncal-Herrero, D. Hall, S. Milne, A. Rappe, D. Sinclair *et al.*, Structural investigation of the temperature-stable relaxor dielectric $Ba_{0.8}Ca_{0.2}TiO_3-Bi(Mg_{0.5}Ti_{0.5})O_3$, J. Eur. Ceram. Soc. **43**, 362 (2023).

[23] V. Krayzman, I. Levin, J. C. Woicik, and F. Bridges, Correlated rattling-ion origins of dielectric properties in reentrant dipole glasses $BaTiO_3-BiScO_3$, Appl. Phys. Lett. **107**, 192903 (2015).

[24] I. Levin, V. Krayzman, J. C. Woicik, F. Bridges, G. E. Sterbinsky, T.-M. Usher, J. L. Jones, and D. Torrejon, Local

structure in $BaTiO_3-BiScO_3$ dipole glasses, Phys. Rev. B **93**, 104106 (2016).

[25] Y.-H. Shin, V. R. Cooper, I. Grinberg, and A. M. Rappe, Development of a bond-valence molecular-dynamics model for complex oxides, Phys. Rev. B **71**, 054104 (2005).

[26] S. Liu, I. Grinberg, H. Takenaka, and A. M. Rappe, Reinterpretation of the bond-valence model with bond order formalism: An improved bond-valence-based interatomic potential for $PbTiO_3$, Phys. Rev. B **88**, 104102 (2013).

[27] I. D. Brown, Recent developments in the methods and applications of the bond valence model, Chem. Rev. **109**, 6858 (2009).

[28] M. Finnis and J. Sinclair, A simple empirical n-body potential for transition metals, Philos. Mag. A **50**, 45 (1984).

[29] M. A. Harvey, S. Baggio, and R. Baggio, A new simplifying approach to molecular geometry description: The vectorial bond-valence model, Acta Crystallogr. B **62**, 1038 (2006).

[30] S. Liu, I. Grinberg, and A. M. Rappe, Development of a bond-valence based interatomic potential for $BiFeO_3$ for accurate molecular dynamics simulations, J. Phys.: Condens. Matter **25**, 102202 (2013).

[31] J. Zhang, Y. Qi, and A. M. Rappe, Developing a force field for the $Ba_{1x}Ca_xZrO_3$ ferroelectric alloy: Prediction of a ferroelectric superlattice structure, Phys. Rev. B **105**, 214204 (2022).

[32] R. B. Wexler, Y. Qi, and A. M. Rappe, Sr-induced dipole scatter in $Ba_xSr_{1x}TiO_3$: Insights from a transferable bond valence-based interatomic potential, Phys. Rev. B **100**, 174109 (2019).

[33] Y. Qi, S. Liu, I. Grinberg, and A. M. Rappe, Atomistic description for temperature-driven phase transitions in $BaTiO_3$, Phys. Rev. B **94**, 134308 (2016).

[34] See Supplemental Material at http://link.aps.org/supplemental/10.1103/PhysRevMaterials.8.014406 for A-site cation controlled localization of dipole correlations in a relaxor material. The Supplemental Material also contains Refs. [60,61].

[35] A. P. Thompson, H. M. Aktulga, R. Berger, D. S. Bolintineanu, W. M. Brown, P. S. Crozier, P. J. in 't Veld, A. Kohlmeyer, S. G. Moore, T. D. Nguyen, R. Shan, M. J. Stevens, J. Tranchida, C. Trott, and S. J. Plimpton, LAMMPS - a flexible simulation tool for particle-based materials modeling at the atomic, meso, and continuum scales, Comput. Phys. Commun. **271**, 108171 (2022).

[36] P. Giannozzi, S. Baroni, N. Bonini, M. Calandra, R. Car, C. Cavazzoni, D. Ceresoli, G. L. Chiarotti, M. Cococcioni, I. Dabo, A. Dal Corso, S. de Gironcoli, S. Fabris, G. Fratesi, R. Gebauer, U. Gerstmann, C. Gougoussis, A. Kokalj, M. Lazzeri, L. Martin-Samos, N. Marzari, F. Mauri, R. Mazzarello, S. Paolini, A. Pasquarello, L. Paulatto, C. Sbraccia, S. Scandolo, G. Sclauzero, A. P. Seitsonen, A. Smogunov, P. Umari, and R. M. Wentzcovitch, Quantum espresso: A modular and open-source software project for quantum simulations of materials, J. Phys.: Condens. Matter **21**, 395502 (2009).

[37] J. P. Perdew, A. Ruzsinszky, C. Gábor, O. A. Vydrov, G. E. Scuseria, L. A. Constantin, X. Zhou, and K. Burke, Restoring the density-gradient expansion for exchange in solids and surfaces, Phys. Rev. Lett. **100**, 136406 (2008).

[38] http://opium.sourceforge.net.

[39] N. J. Ramer and A. M. Rappe, Designed nonlocal pseudopotentials for enhanced transferability, Phys. Rev. B **59**, 12471 (1999).

[40] A. M. Rappe, K. M. Rabe, E. Kaxiras, and J. D. Joannopoulos, Optimized pseudopotentials, Phys. Rev. B **41**, 1227 (1990).

[41] H. J. Monkhorst and J. D. Pack, Special points for brillouin-zone integrations, Phys. Rev. B **13**, 5188 (1976).

[42] M. Parrinello and A. Rahman, Crystal structure and pair potentials: A molecular-dynamics study, Phys. Rev. Lett. **45**, 1196 (1980).

[43] S. Nośe, Constant-temperature molecular dynamics, J. Phys.: Condens. Matter **2**, SA115 (1990).

[44] W. G. Hoover and B. L. Holian, Kinetic moments method for the canonical ensemble distribution, Phys. Lett. A **211**, 253 (1996).

[45] J. Caillol, D. Levesque, and J. Weis, Theoretical calculation of ionic solution properties, J. Chem. Phys. **85**, 6645 (1986).

[46] I. Ponomareva, L. Bellaiche, and R. Resta, Dielectric anomalies in ferroelectric nanostructures, Phys. Rev. Lett. **99**, 227601 (2007).

[47] S. Liu and R. E. Cohen, Origin of stationary domain wall enhanced ferroelectric susceptibility, Phys. Rev. B **95**, 094102 (2017).

[48] X. Gonze, D. C. Allan, and M. P. Teter, Dielectric tensor, effective charges, and phonons in α-quartz by variational density functional perturbation theory, Phys. Rev. Lett. **68**, 3603 (1992).

[49] A. Zeb and S. J. Milne, Stability of high-temperature dielectric properties for (1- x) $Ba_{0.8}Ca_{0.2}TiO_3$-x Bi $(Mg_{0.5}Ti_{0.5})O_3$ ceramics, J. Am. Ceram. Soc. **96**, 2887 (2013).

[50] Q. Zhang, Z. Li, F. Li, and Z. Xu, Structural and dielectric properties of Bi $(Mg_{1/2}Ti_{1/2})O_3$-$BaTiO_3$ lead-free ceramics, J. Am. Ceram. Soc. **94**, 4335 (2011).

[51] A. Glazounov, A. Bell, and A. Tagantsev, Relaxors as superparaelectrics with distributions of the local transition temperature, J. Phys.: Condens. Matter **7**, 4145 (1995).

[52] R. K. Pattnaik, J. Toulouse, and B. George, Relaxation of li-dipole pairs in the disordered perovskite $K_{1x}Li_xTaO_3$ and the effect of external electric fields, Phys. Rev. B **62**, 12820 (2000).

[53] R. D. Shannon, Revised effective ionic radii and systematic studies of interatomic distances in halides and chalcogenides, Acta. Cryst. A **32**, 751 (1976).

[54] M. Čebela, D. Zagorac, K. Batalović, J. Radaković, B. Stojadinović, V. Spasojević, and R. Hercigonja, $BiFeO_3$ perovskites: A multidisciplinary approach to multiferroics, Ceram. Int. **43**, 1256 (2017).

[55] W. J. Merz, The electric and optical behavior of $BaTiO_3$ single-domain crystals, Phys. Rev. **76**, 1221 (1949).

[56] D. C. Arnold, K. S. Knight, F. D. Morrison, and P. Lightfoot, The ferroelectric-paraelectric phase transition in $BiFeO_3$: Crystal structure of the orthorhombic beta-phase, Phys. Rev. Lett. **102**, 027602 (2009).

[57] J. Shi, I. Grinberg, X. Wang, and A. M. Rappe, Atomic sublattice decomposition of piezoelectric response in tetragonal $PbTiO_3$, $BaTiO_3$, and $KnBO_3$, Phys. Rev. B **89**, 094105 (2014).

[58] I. Grinberg, M. R. Suchomel, P. K. Davies, and A. M. Rappe, Predicting morphotropic phase boundary locations and transition temperatures in Pb- and Bi-based perovskite solid solutions from crystal chemical data and first-principles calculations, J. Appl. Phys. **98**, 094111 (2005).

[59] A. Samanta, S. Yadav, Z. Gu, C. J. Meyers, L. Wu, D. Chen, S. Pandya, R. A. York, L. W. Martin, J. E. Spanier *et al.*, A predictive theory for domain walls in oxide ferroelectrics based on interatomic interactions and its implications for collective material properties, Adv. Mater. **34**, 2106021 (2022).

[60] I. Brown and R. Shannon, Empirical bond-strengthbond-length curves for oxides, Acta Cryst. A **29**, 266 (1973).

[61] I. Brown and K. K. Wu, Empirical parameters for calculating cation-oxygen bond valences, Acta. Cryst. B **32**, 1957 (1976).